Catalysis Science & Technology

PAPER

View Article Online
View Journal | View Issue

Cite this: *Catal. Sci. Technol.*, 2015, 5, 979

Synergistic effects of Ni and Cu supported on TiO_2 and SiO_2 on photocatalytic H_2 evolution with an electron donor–acceptor linked molecule†

Yusuke Yamada,*[a] Shinya Shikano,[a] Tomoki Akita[b] and Shunichi Fukuzumi*[a]

Synergistic effects of Ni and Cu supported on metal oxides on their catalytic activity for hydrogen evolution were observed in photocatalytic hydrogen evolution with 2-phenyl-4-(1-naphthyl)quinolinium ion ($QuPh^+$–NA) and β-dihydronicotinamide adenine dinucleotide (NADH) as a photocatalyst and an electron donor, respectively. Among the catalysts of Ni and Cu supported on TiO_2, SiO_2, SiO_2–Al_2O_3 and CeO_2, Ni and Cu supported on TiO_2 and SiO_2 exhibited high catalytic activity at a wide range of Ni contents [Ni/(Ni + Cu)] from 30% to 70%, while Ni or Cu solely supported on TiO_2 and SiO_2 showed insignificant catalytic activity. The catalytic activity of Ni and Cu supported on TiO_2 and SiO_2 depends on the preparation methods of the catalysts. The catalysts prepared by a co-impregnation method, in which a precursor solution containing both $Ni(NO_3)_2$ and $Cu(NO_3)_2$ was used for the impregnation, showed high catalytic activity, whilst catalysts prepared by a sequential impregnation method, in which $Ni(NO_3)_2$ and $Cu(NO_3)_2$ were loaded and calcined successively, exhibited low catalytic activity. TEM observations with energy-dispersive X-ray spectroscopy (EDS) elemental mapping of these catalysts revealed that Ni and Cu were closely located on the support surfaces of a catalyst prepared by the co-impregnation method, whereas Ni and Cu were separated in the catalyst prepared by the sequential impregnation method. These results suggest that the close location of Ni and Cu is necessary to exhibit the high catalytic activity. Such a synergistic effect among base metals and metal oxide supports would be a key to develop active catalysts for hydrogen evolution without using platinum group metals.

Received 31st August 2014,
Accepted 2nd October 2014

DOI: 10.1039/c4cy01128g

www.rsc.org/catalysis

Introduction

Hydrogen (H_2) production utilising solar energy attracts much attention from the viewpoint of storage of natural energy as chemical energy.[1–11] A photocatalytic H_2 evolution system, which mimics natural photosynthesis, can be constructed by using an electron donor, a photosensitiser, an electron mediator and an H_2 evolution catalyst.[12–20] For example, H_2 evolution can be observed by the photoirradiation of a solution containing ethylenediaminetetraacetic acid disodium salt, $[Ru(bpy)_3]^{2+}$ (bpy = 2,2′-bipyridine), methyl viologen and Pt particles as an electron donor, a photosensitiser, an electron mediator and a hydrogen evolution catalyst, respectively.[21] This type of H_2 evolution systems requires a sacrificial electron donor; however, a high quantum efficiency and rational improvement in catalysis are achievable by replacing each component after modification.[8,22,23] As a component of an H_2 evolution catalyst, Pt particles have been most widely used because of their very low overpotential for proton reduction.[24–26] However, avoiding or reducing the use of Pt metal is strongly demanded because of its high cost and limited supply.[22,27]

Alternative to Pt nanoparticles (PtNPs), Ru nanoparticles (RuNPs) and Ni nanoparticles (NiNPs) have been demonstrated to act as H_2 evolution catalysts in reaction systems using organic electron donor–acceptor linked dyads as photocatalysts.[28,29] RuNPs exhibit virtually the same activity as PtNPs; however, the catalytic activity of NiNPs was lower than those of PtNPs and RuNPs.[28–30] For the improvement of Ni catalysis, concomitant use of other metals such as Cu, Pd and Co is promising as reported for various catalytic reactions.[31–33] For example, Ni–Cu alloy nanoparticles have been reported to exhibit catalytic activity for thermal H_2 evolution by hydrolysis of sodium borohydride higher than nanoparticles solely composed of Ni or Cu.[34] Such a synergistic effect between Ni and Cu has also been reported for

[a] *Department of Material and Life Science, Graduate School of Engineering, Osaka University, ALCA, Japan Science and Technology Agency (JST), Suita, Osaka 565-0871, Japan. E-mail: fukuzumi@chem.eng.osaka-u.ac.jp, yamada@chem.eng.osaka-u.ac.jp*

[b] *National Institute of Advanced Industrial Science and Technology (AIST), Ikeda, Osaka 563-8577, Japan*

† Electronic supplementary information (ESI) available: Time courses of H_2 evolution (Fig. S1, S4 and S8), powder X-ray diffraction (Fig. S2, S5 and S9), the amount of H_2 evolved in the repetitive experiments (Fig. S3), diffused reflectance spectra (Fig. S6), and TEM images (Fig. S7). See DOI: 10.1039/c4cy01128g

supporting catalysts using SiO_2,[35] Al_2O_3,[36–38] CeO_2,[39] ZrO_2[40] and TiO_2[41] for high-temperature reactions such as ethanol steam reforming. In general, supporting catalytically active metals on a metal oxide is beneficial for improvements not only in the catalytic activity by metal–support interaction but also in the durability of the metal nanoparticles. However, there have been no systematic studies on the synergistic and support effects of Ni and Cu catalysts on photocatalytic H_2 evolution.

We report herein the H_2 evolution catalysis of Ni–Cu/TiO_2 and Ni–Cu/SiO_2 in an efficient photocatalytic H_2 evolution system composed of a donor–acceptor linked dyad, 2-phenyl-4-(1-naphthyl)quinolinium ion ($QuPh^+$–NA), as a photocatalyst and β-dihydronicotinamide adenine dinucleotide (NADH) as a sacrificial electron donor. The chemical structure of the organic photocatalyst used in this study and the overall reaction scheme are shown in Scheme 1. Upon photoexcitation of $QuPh^+$–NA, electron transfer from the NA moiety to the singlet excited state of the $QuPh^+$ moiety occurs to produce the electron-transfer state ($QuPh^{\bullet}$–$NA^{\bullet+}$).[42,43] Then, electron transfer from NADH to $QuPh^{\bullet}$–$NA^{\bullet+}$ occurs to produce $NADH^{\bullet+}$ and $QuPh^{\bullet}$–NA.[28] $NADH^{\bullet+}$ undergoes deprotonation, releasing one proton to afford $NAD^{\bullet}$ that can transfer an electron to $QuPh^+$–NA to produce NAD^+ and $QuPh^{\bullet}$–NA.[28] Two equivalents of $QuPh^{\bullet}$–NA thus produced can inject two electrons to Ni–Cu catalysts to evolve H_2 from two protons.[28] It should be noted that no electron mediator, which is frequently used in homogeneous photocatalytic H_2 production, is required in the present photocatalytic system because the electron-transfer state of $QuPh^+$–NA has a sufficient lifetime for the oxidation of NADH and also for electron injection to Ni–Cu catalysts.[25,28–30] In this reaction system, effects of the Ni/Cu ratio, preparation methods, the surface area and morphology of SiO_2, and the surface area and crystal structure of TiO_2 on the catalysis of Ni–Cu/TiO_2 and Ni–Cu/SiO_2 for H_2 evolution were examined to clarify the conditions to achieve the synergistic and support effect, which would be a key to develop active catalysts alternative to platinum group metals.

2. Results and discussion

2.1 Photocatalytic H_2 evolution with Ni and a transition metal supported on metal oxides

The effect of concomitant use of Ni with another metal, Cu, Co or Fe, supported on TiO_2 or SiO_2 was examined on the H_2 evolution catalysis of Ni. These catalysts were prepared by a co-impregnation method. Photocatalytic H_2 evolution was performed by photoirradiation ($\lambda > 340$ nm) of a mixed suspension (2.0 mL) of MeCN and a phthalate buffer (pH 4.5) [1 : 1 (v/v)] containing $QuPh^+$–NA (8.8×10^{-4} M), NADH (1.0×10^{-3} M) and TiO_2 or SiO_2 supporting Ni and another metal (M) (100 mg L^{-1}, M = Cu, Co or Fe), in which the loading amount was 1.5 wt% for each of Ni and M, as shown in Fig. 1.

A significant amount of H_2 evolution was observed only for Ni–Cu/TiO_2. TiO_2 is a well-known photocatalyst; however, no H_2 evolution was confirmed for a reaction suspension without $QuPh^+$–NA under the present reaction conditions (Fig. S1a†). From the reaction suspension using Ni–Cu/TiO_2 as an H_2 evolution catalyst in the presence of $QuPh^+$–NA, continuous H_2 evolution was observed after a short induction period for *ca.* 5 min. This induction period is for the reduction of NiO, $NiCuO_2$ and/or Cu_2O species to be catalytically active metallic species because the presence of NiO (JCPDS card no. 78-0643) species in as-prepared Ni–Cu/TiO_2 was confirmed by the diffraction peak around $2\theta = 43.4°$ in the powder X-ray diffraction (Fig. 2). This peak may overlap with the diffraction peaks from $NiCuO_2$ (JCPDS card no. 6-720) and Cu_2O (JCPDS card no. 05-0667), which have been reported to provide the diffraction peaks at $2\theta = 43.8°$ and 42.5°, respectively, because no diffraction peak was observed at $2\theta = 35.6°$, which indicates formation of CuO (JCPDS card no. 05-0661). Powder XRD measurements were also performed for the Ni–Cu/TiO_2 after the photocatalytic reaction. No diffraction peak indicating formation of Ni^0 or Cu^0 species was clearly observed in the peak that appeared around 43° (Fig. S2†).

The initial H_2 evolution rate for the reaction system using Ni–Cu/TiO_2 was determined to be 1.7 μmol h^{-1} from the initial (45 min) slope of the reaction system. The apparent quantum yield obtained under photoirradiation ($\lambda = 350 \pm 10$ nm) for 1 h was 1.1%, where the photon flux determined by using an actinometer was 2.89×10^{-9} einstein s^{-1}. The rate was 10 times slower compared with the H_2 evolution rate determined for the reaction system using Pt nanoparticles instead of Ni–Cu/TiO_2, in which the weight of used Pt was the same as that of Ni–Cu in the Ni–Cu/TiO_2; however, the maximum H_2 yield based on the amount of NADH reached as high as 87% (1.7 μmol) without using precious metals.

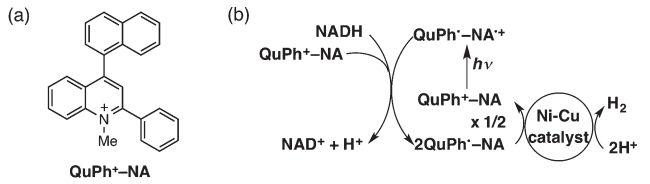

Scheme 1 (a) Structure of $QuPh^+$–NA and (b) the overall photocatalytic cycle for H_2 evolution using $QuPh^+$–NA and an Ni–Cu catalyst.

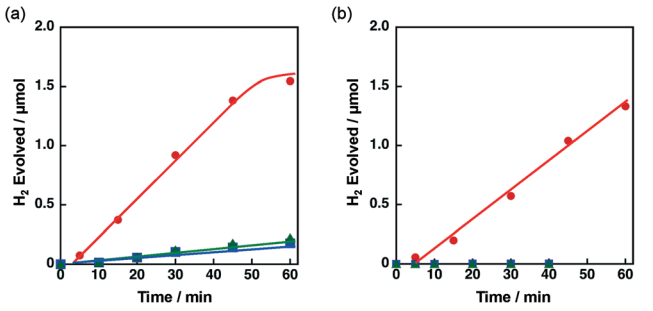

Fig. 1 Time courses of H_2 evolution by photoirradiation ($\lambda > 340$ nm) of a mixed suspension (2.0 mL) of a phthalate buffer (pH 4.5) and MeCN [1 : 1 (v/v)] containing $QuPh^+$–NA (8.8×10^{-4} M), NADH (1.0×10^{-3} M) and (a) 3 wt% Ni–M/TiO_2 or (b) 3 wt% Ni–M/SiO_2 (100 mg L^{-1}, M = Cu (red circle), Co (green triangle) and Fe (blue square)).

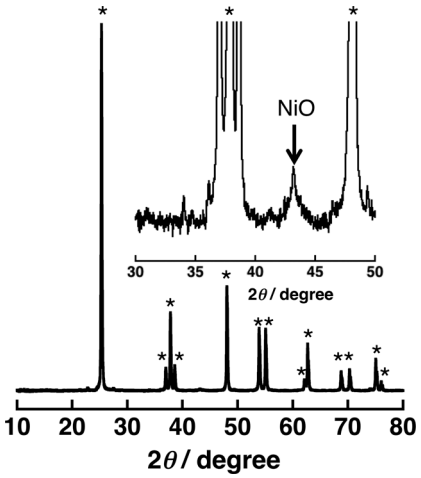

Fig. 2 Powder X-ray diffraction patterns of 3 wt% Ni–Cu/TiO_2 [Ni/Cu = 1 : 1 (w/w)]. The peaks with the asterisk symbol (*) originate from TiO_2 (anatase).

Ceasing H_2 evolution by cutting off the light in the course of the reaction ensures that the H_2 evolution proceeds photocatalytically (Fig. S1b†). In addition, a photocatalytic system using a reduced amount of $QuPh^+$–NA (0.11 mM) repeatedly evolved H_2 five times by the addition of NADH to the reaction solution after ceasing H_2 evolution (Fig. S3†), and the turnover number based on $QuPh^+$–NA reached 21. On the other hand, the amount of H_2 evolution was less than 0.1 μmol from the suspensions containing TiO_2 supporting Ni–Fe and Ni–Co as H_2 evolution catalysts by photoirradiation for 60 min (Fig. 1a, green triangle and blue square, respectively). Similarly, a negligible amount of H_2 evolution was observed from the reaction suspensions containing Ni/TiO_2 and Cu/TiO_2 as the H_2 evolution catalysts (Fig. S4a†). Thus, Cu acts as the only suitable counterpart of Ni to achieve synergistic effects on the H_2 evolution catalysis.

Similar synergistic effects of Ni and Cu on the photocatalytic H_2 evolution were observed for Ni–Cu/SiO_2 as shown in Fig. 1b, in which the maximum H_2 yield reached 77% (1.5 μmol) with a H_2 evolution rate of 1.3 μmol h^{-1} determined from the initial (60 min) slope. No H_2 evolution was confirmed for Ni–Fe/SiO_2 and Ni–Co/SiO_2 by photoirradiation for 40 min. An insignificant amount of H_2 evolution was observed from the reaction suspensions employing Ni/SiO_2 and Cu/SiO_2 as the H_2 evolution catalysts (Fig. S4b†). These results obviously indicate that addition of Cu is effective to improve the catalysis of Ni supported on both TiO_2 and SiO_2, although the addition of Fe or Co was unprofitable.

Support effects on the catalytic activity of Ni–Cu catalysts were also examined by employing TiO_2, SiO_2, SiO_2–Al_2O_3 and CeO_2 as supports. Ni and Cu were loaded on the supports by a co-impregnation method where the loading amount was 1.5 wt% for each Cu and Ni. The Brunauer–Emmett–Teller (BET) surface areas of TiO_2, SiO_2, SiO_2–Al_2O_3, and CeO_2 were determined to be 6.8, 52, 118 and 162 m^2 g^{-1}, respectively. The surface area of the TiO_2 is significantly low compared to those of others; however, the effect of surface area on the catalytic activity of Ni–Cu/TiO_2 is limited (*vide infra*, Fig. 12). Powder X-ray diffraction patterns of these metal oxides suggested that SiO_2 and SiO_2–Al_2O_3 are amorphous in nature, whilst TiO_2 and CeO_2 are crystalline in the anatase and fluorite structures, respectively (Fig. S5†). These metal oxide supports were chosen from those often used for supporting Ni for various reactions.[39–41] As mentioned above, both TiO_2 and SiO_2 supporting Ni–Cu showed high catalytic activity in terms of both H_2 yields and H_2 evolution rates (dashed lines in Fig. 3) in the photocatalytic H_2 evolution. On the other hand, Ni–Cu supported on SiO_2–Al_2O_3 (red triangle) and CeO_2 (blue inverted triangle) showed no significant activity for the photocatalytic H_2 evolution as shown in Fig. 3. Although the origin of the support effect is still unclear, the readily reducible nature may be beneficial to produce active sites at the perimeter between Ni–Cu species and the supports. The small negative standard enthalpies of formation for TiO_2 and SiO_2 (−940 and −910 kJ mol^{-1}, respectively) compared to those for CeO_2 and Al_2O_3 (−1089 and −1676 kJ mol^{-1}, respectively) suggest that TiO_2 and SiO_2 are more readily reducible than CeO_2 and SiO_2–Al_2O_3.[44] Thus, SiO_2 and TiO_2 could be suitable supports to achieve Ni–Cu species that are active for photocatalytic H_2 evolution.

2.2 Effect of preparation methods on H_2 evolution catalysis of Ni–Cu supported on TiO_2 and SiO_2

The catalytic activity of Ni–Cu/TiO_2 and Ni–Cu/SiO_2 was highly influenced by preparation methods. When Ni–Cu/TiO_2 prepared by a co-impregnation method using a solution containing both $Cu(NO_3)_2$ and $Ni(NO_3)_2$ was examined for the photocatalytic H_2 evolution, a fast H_2 evolution rate was observed (Fig. 1a, 1.7 μmol h^{-1}). On the other hand, the H_2 evolution rates were as low as 0.5 and 0.3 μmol h^{-1} with catalysts prepared by a sequential impregnation method, in

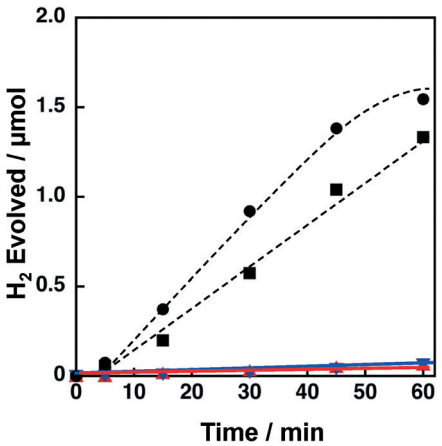

Fig. 3 Time courses of H_2 evolution by photoirradiation ($\lambda > 340$ nm) of a mixed suspension (2.0 mL) of a phthalate buffer (pH 4.5) and MeCN [1 : 1 (v/v)] containing $QuPh^+$–NA (8.8×10^{-4} M), NADH (1.0×10^{-3} M) and 3 wt% Ni–Cu/MO_x (100 mg L^{-1}, MO_x = TiO_2, circle; SiO_2, square; SiO_2–Al_2O_3, red triangle; CeO_2, blue inverted triangle).

which Ni/TiO_2 was impregnated with a $Cu(NO_3)_2$ solution or Cu/TiO_2 with a $Ni(NO_3)_2$ solution (red circle and blue square in Fig. 4a, respectively). Similar influence of preparation methods was also observed for $Ni–Cu/SiO_2$ as shown in Fig. 4b. The H_2 evolution rate obtained for $Ni–Cu/SiO_2$ prepared by co-impregnation was significantly larger (Fig. 1b, 1.3 μmol h^{-1}) than those obtained for $Ni–Cu/SiO_2$ catalysts prepared by the sequential impregnation method, 0.1 and 0.2 μmol h^{-1}.

2.3 Characterisation of Ni–Cu supported on TiO_2 and SiO_2 by UV-vis and TEM with EDS elemental mapping

The $Ni–Cu/TiO_2$ and $Ni–Cu/SiO_2$ catalysts prepared by co-impregnation and sequential impregnation methods were characterised by diffuse reflectance UV-vis spectroscopy (DRS). The DRS results of $Ni–Cu/TiO_2$ catalysts prepared by different procedures are shown in Fig. 5a. $Ni–Cu/TiO_2$ prepared by the co-impregnation method (red) showed strong absorption in the visible region (400–800 nm) compared with $Ni–Cu/TiO_2$ catalysts prepared by the sequential impregnation method, with the Cu loaded on Ni/TiO_2 (blue) or Ni loaded on Cu/TiO_2 (green). The peaks that appeared around 600–800 nm in the DRS of $Ni–Cu/TiO_2$ catalysts differ from superposition of DRS of Ni/TiO_2 and Cu/TiO_2 depicted in Fig. S6a,† suggesting that a part of Ni and Cu species have electronic interaction on the TiO_2 surfaces.

A more obvious difference in DRS was observed among $Ni–Cu/SiO_2$ catalysts prepared by different methods as shown in Fig. 5b. The DRS results of Ni/SiO_2 and Cu/SiO_2 are depicted in Fig. S6b.† The DRS of the $Ni–Cu/SiO_2$ catalyst prepared by the co-impregnation method (red) showed absorption maxima around 480 nm, whereas a small shoulder around 400 nm was observed for the $Ni–Cu/SiO_2$ catalysts prepared by the sequential impregnation method. The difference in the absorption at the visible region provides the difference in colour. The origin of the brownish colour of the $Ni–Cu/SiO_2$ catalyst prepared by the co-impregnation method

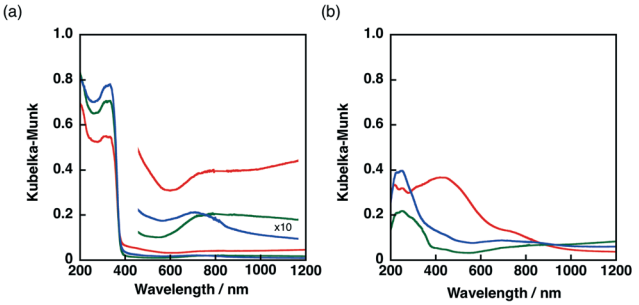

Fig. 5 Diffuse reflectance UV-vis spectra of (a) $Ni–Cu/TiO_2$ and (b) $Ni–Cu/SiO_2$ catalysts prepared by co-impregnation (red) and sequential impregnation methods (Cu loaded on Ni/MO_2, blue, and Ni loaded on Cu/MO_2, green. M = Ti or Si).

can be ascribed to the formation of $NiCuO_2$ on SiO_2 surfaces, which has been proposed for Ni–Cu supported on cordierite in the literature.[45]

The difference in the structures of the $Ni–Cu/SiO_2$ catalysts prepared by the co-impregnation and the sequential impregnation methods was confirmed by TEM measurements in the atomic level with the energy-dispersive X-ray spectroscopy (EDS) elemental mapping for Si, Cu and Ni. Fig. 6 shows a high-angle annular dark-field scanning TEM (HAADF-STEM) image of particles 20 nm in size formed on $Ni–Cu/SiO_2$ prepared by the co-impregnation method. The EDS elemental mapping for Si (blue), Cu (red) and Ni (green) indicates that the particle observed in the HAADF-STEM image is composed of both Cu and Ni. On the other hand, the particles on $Ni–Cu/SiO_2$ prepared by the sequential method, in which Cu was loaded on Ni/SiO_2, showed separated deposition of Cu and Ni. As shown in Fig. 7, comparison of EDS elemental

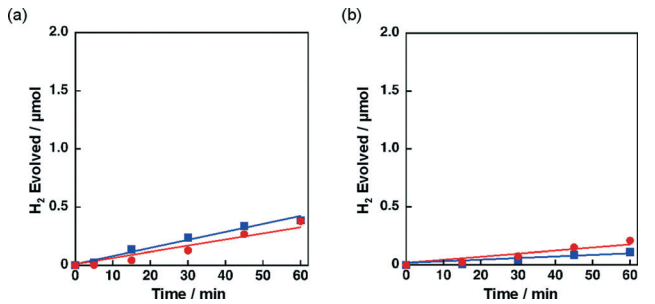

Fig. 4 Time courses of H_2 evolution by photoirradiation ($\lambda > 340$ nm) of a mixed suspension (2.0 mL) of a phthalate buffer (pH 4.5) and MeCN [1:1 (v/v)] containing $QuPh^+$–NA (8.8×10^{-4} M), NADH (1.0×10^{-3} M) and (a) 3 wt% $Ni–Cu/TiO_2$ (100 mg L^{-1}) prepared by a sequential impregnation method (Cu loaded on Ni/TiO_2, red circle, and Ni loaded on Cu/TiO_2, blue square) and (b) 3 wt% $Ni–Cu/SiO_2$ catalysts (100 mg L^{-1}) prepared by a sequential impregnation (Cu loaded on Ni/SiO_2, red circle, and Ni loaded on Cu/SiO_2, blue square).

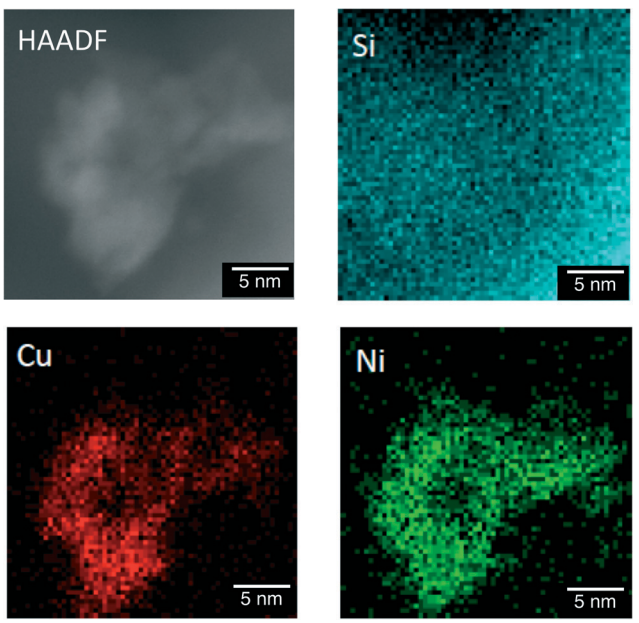

Fig. 6 HAADF-STEM and energy-dispersive X-ray spectroscopy (EDS) elemental mapping of $Ni–Cu/SiO_2$ prepared by the co-impregnation method for Si, Cu and Ni.

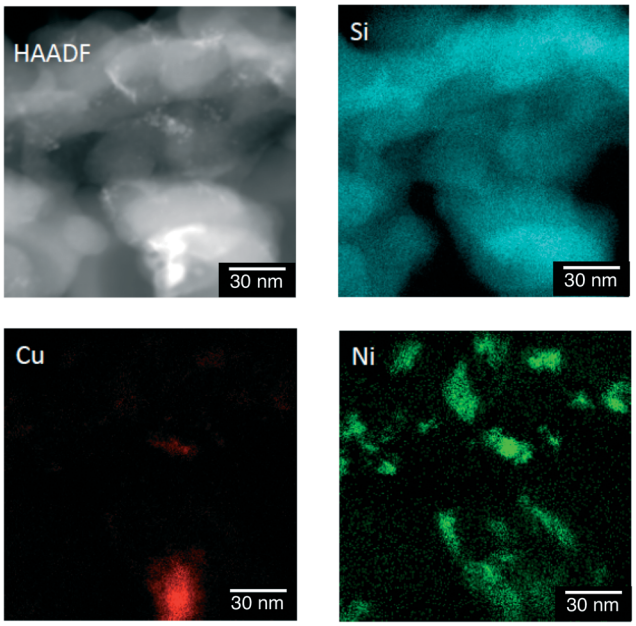

Fig. 7 HAADF-STEM and EDS elemental mapping of Ni–Cu/SiO_2 prepared by the sequential impregnation method (Ni loaded on Cu/SiO_2) for Si, Cu and Ni.

mapping for Cu (red) and Ni (green) with the HAADF-STEM image indicates that the brightest part of the HAADF-STEM image is the Cu-rich region, and the small particles that appeared in the upper middle are Ni rich or Ni only. These observations suggest that suitable selection of preparation methods is necessary to achieve close location of Ni and Cu on the surfaces of Ni–Cu/SiO_2.

2.4 Optimisation of Ni/Cu ratio, loading amount of Ni–Cu and structure of TiO_2 and SiO_2 supports

The catalytic activity of Ni–Cu/SiO_2 with different loading amounts of Ni–Cu [1 : 1 (w/w)] ranging from 2 to 5 wt% was examined for the photocatalytic H_2 evolution. The H_2 evolution rates determined from the slopes of time courses of H_2 evolution (Fig. 8a) at the reaction time from 5 to 30 min were 0.8, 1.2, 1.3 and 1.0 μmol h^{-1} for Ni–Cu/SiO_2 with the loading amounts of Ni–Cu being 2, 3, 4 and 5 wt%, respectively. The total H_2 yield obtained for 3 wt% Ni–Cu/SiO_2 was 77%, which is higher than those for 2, 4 and 5 wt% Ni–Cu/SiO_2 (28%, 54% and 45%, respectively). Thus, the loading amount of Ni–Cu around 3–4 wt% is optimum to achieve high catalytic activity for Ni–Cu/SiO_2.

The effect of the ratio between Ni and Cu on the catalytic activity of 3 wt% Ni–Cu/SiO_2 was also examined. Fig. 9a shows the time courses of H_2 evolution in the photocatalytic H_2 evolution using Ni–Cu/SiO_2 catalysts with Ni contents, the Ni/(Ni + Cu) ratio, from 0% to 100%. H_2 evolution rates higher than 0.8 μmol h^{-1} were observed for the catalysts with Ni contents from 25% to 67% as shown in Fig. 9b. The effect of Cu on the reducibility of NiO on SiO_2 has been discussed by temperature-programmed reaction with flowing H_2/Ar in the literature.[35c–e] The reduction temperature of NiO on SiO_2 around 580 °C decreased to below 300 °C for Ni–Cu/SiO_2 under 10% flowing H_2/Ar.[35c] The enhanced reducibility of NiO on Ni–Cu/SiO_2 catalysts resulted in high catalytic activity for ethanol steam reforming.[35c] The promotional effect of Cu(O) on the reduction of NiO can also be expected for the present photocatalytic H_2 evolution system, although the reaction temperature was as low as room temperature.

Effects of the morphologies and the surface areas of SiO_2 supports on the catalysis of Ni–Cu/SiO_2 for H_2 evolution were also examined by employing two additional SiO_2 supports, which have a spherical morphology with the BET surface area similar to that of the SiO_2 support [unshaped, low surface area (unshaped LS)] used in the above experiments and an unshaped morphology with a higher BET surface area. The morphologies of SiO_2 supports were confirmed by TEM observations as shown in Fig. S7,† and the BET surface areas were determined to be 59 m^2 g^{-1} and 420 m^2 g^{-1} for the SiO_2 (spherical) and the SiO_2 [unshaped, high surface area (unshaped HS)], respectively. With these SiO_2 supports, 3 wt% Ni–Cu/SiO_2 catalysts [Ni/Cu = 1 : 1 (w/w)] were prepared by the co-impregnation method and used as the H_2 evolution

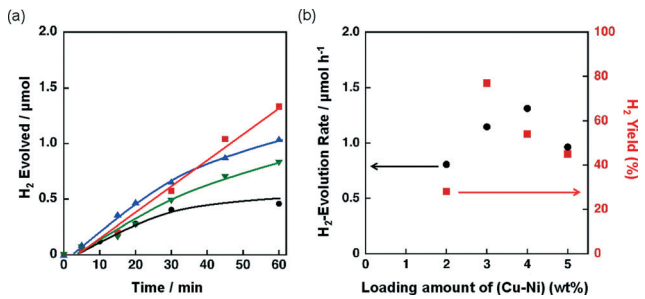

Fig. 8 (a) Time course of H_2 evolution by photoirradiation ($\lambda > 340$ nm) of a mixed suspension (2.0 mL) of a phthalate buffer (pH 4.5) and MeCN [1 : 1 (v/v)] containing $QuPh^+$–NA (8.8×10^{-4} M), NADH (1.0×10^{-3} M) and Ni–Cu/SiO_2 [Ni/Cu = 1/1 (w/w)] (100 mg L^{-1}; 2 wt%, black circle; 3 wt%, red square; 4 wt%, blue triangle; 5 wt%, inverted triangle) prepared by co-impregnation. (b) Effect of the loading amount of Cu and Ni on the initial (30 min) H_2 evolution rate and H_2 yield.

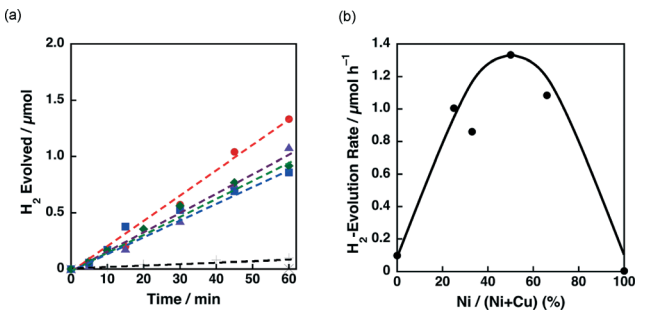

Fig. 9 (a) Time courses of H_2 evolution by photoirradiation ($\lambda > 340$ nm) of a mixed suspension (2.0 mL) of a phthalate buffer (pH 4.5) and MeCN [1 : 1 (v/v)] containing $QuPh^+$–NA (8.8×10^{-4} M), NADH (1.0×10^{-3} M) and 3 wt% Ni–Cu/SiO_2 (100 mg L^{-1}) with various Ni contents prepared by the co-impregnation method [Ni/(Ni + Cu) = 0% (plus), 25% (green diamond), 33% (blue square), 50% (red circle), 67% (purple triangle) and 100% (inverted triangle)]. (b) Plot of the initial H_2 evolution rate *vs.* Ni contents.

catalysts in the photocatalytic H_2 evolution system. The time courses of the H_2 evolution are shown in Fig. 10a. The H_2 evolution rates were 0.4 and 0.8 μmol h^{-1} for Ni–Cu/SiO_2 catalysts with spherical and unshaped (high surface area) morphologies, respectively. The H_2 evolution rate for Ni–Cu/SiO_2 (spherical) being significantly lower than that for Ni–Cu/SiO_2 [unshaped LS (52 m^2 g^{-1})] (1.3 μmol h^{-1}) indicates that the morphology of SiO_2 affects the catalysis of Ni–Cu/SiO_2. The lower catalytic activity obtained by employing SiO_2 (spherical) as a support has been reported for Ru/SiO_2 in the photocatalytic H_2 evolution.[30] The smooth surfaces of the SiO_2 (spherical) more readily promote the adhesive interaction among the SiO_2 particles through supporting metals than the rough surfaces of the SiO_2 (unshaped).[30] Thus, a part of the supporting metals acting as the adhesive among SiO_2 particles hardly work as the H_2 evolution catalyst. A similar mechanism is applicable to the present Ni–Cu/SiO_2 (spherical) catalysts. For the effects of surface areas, the catalytic activity of Ni–Cu/SiO_2 (unshaped LS) was higher than that of Ni–Cu/SiO_2 (unshaped HS). This result may suggest that the lower surface area of the SiO_2 is favourable to closely locate Ni and Cu to each other. Thus, both morphologies and surface areas of SiO_2 supports affect the catalysis of Ni–Cu/SiO_2.

The effect of the ratio between Ni and Cu was also investigated for 3 wt% Ni–Cu/SiO_2 (spherical) and 3 wt% Ni–Cu/SiO_2 (unshaped HS) in the photocatalytic H_2 evolution. The time courses of the H_2 evolution in the photocatalytic H_2 evolution are shown in Fig. S8.† Fig. 10b shows the relative H_2 evolution rates depending on the Ni/(Ni + Cu). High catalytic activity was achieved at the Ni contents between 30% and 67% as observed for Ni–Cu/SiO_2 (unshaped LS) shown in Fig. 9b.

The catalytic activity of Ni–Cu/TiO_2 for the H_2 evolution dependent on the Ni contents was also investigated in the photocatalytic H_2 evolution. Fig. 11a demonstrates the time courses of H_2 evolution in the photocatalytic reaction systems using Ni–Cu/TiO_2 with different Ni contents. H_2 evolution rates higher than 1.5 μmol h^{-1} were obtained for the Ni–Cu/TiO_2 catalysts with 33–67% of Ni contents. The origin of the

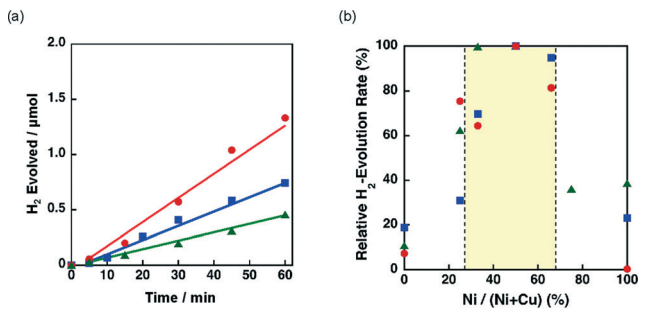

Fig. 10 (a) Time course of H_2 evolution by photoirradiation ($\lambda > 340$ nm) of a mixed suspension (2.0 mL) of a phthalate buffer (pH 4.5) and MeCN [1 : 1 (v/v)] containing $QuPh^+$–NA (8.8×10^{-4} M), NADH (1.0×10^{-3} M) and 3 wt% Ni–Cu/SiO_2 (100 mg L^{-1}). (a) SiO_2 with a spherical morphology (green triangle) and unshaped LS (red circle) and unshaped HS (blue square). (b) Plot of the initial H_2 evolution rate *vs.* Ni contents.

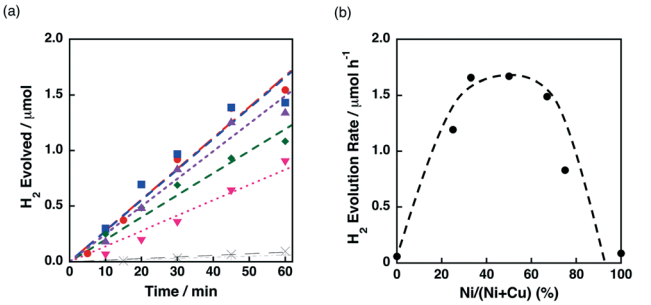

Fig. 11 (a) Time course of H_2 evolution by photoirradiation ($\lambda > 340$ nm) of a mixed suspension (2.0 mL) of a phthalate buffer (pH 4.5) and MeCN [1 : 1 (v/v)] containing $QuPh^+$–NA (8.8×10^{-4} M), NADH (1.0×10^{-3} M) and 3 wt% Ni–Cu/TiO_2 (100 mg L^{-1}) with various Ni contents prepared by co-impregnation [Ni/(Ni + Cu) = 0% (plus), 25% (green diamond), 33% (blue square), 50% (red circle), 67% (purple triangle), 75% (pink inverted triangle) and 100% (cross)]. (b) Plot of the initial H_2 evolution rate *vs.* Ni contents.

synergistic effect of Ni and Cu on TiO_2 has been discussed by H_2-TPR measurements in the literature.[41a] The reduction temperature of NiO on TiO_2 was lowered from *ca.* 500 °C to 300 °C in the presence of CuO by increasing the content of CuO.[41a] Although the photocatalytic H_2 evolution was performed at room temperature, the readily reducible nature of NiO influenced by the addition of Cu would be beneficial to form metallic Ni species on the TiO_2 support.

Effects of crystal structures and the BET surface areas of TiO_2 supports were examined by using a series of 3 wt% Ni–Cu/TiO_2 catalysts in the photocatalytic H_2 evolution. The crystal structures confirmed by XRD (Fig. S9†) and BET surface areas of the TiO_2 supports were rutile with a high surface area (rutile HS, 250 m^2 g^{-1}), rutile with a low surface area (rutile LS, 0.3 m^2 g^{-1}) and anatase with a high surface area (anatase HS, 46 m^2 g^{-1}). The TiO_2 support used in the above-mentioned experiments has an anatase structure with a low surface area (anatase LS, 6.8 m^2 g^{-1}) (*vide supra*). With these TiO_2 supports, 3 wt% Ni–Cu/TiO_2 [Ni/Cu = 1 : 1 (w/w)] catalysts were prepared by the co-impregnation method. Fig. 12 shows the time courses of H_2 evolution in the photocatalytic H_2 evolution performed with these Ni–Cu/TiO_2 catalysts (rutile HS, rutile LS, and anatase HS) as the H_2 evolution catalysts. The H_2 evolution rates determined from the initial (60 min) slopes were 1.5, 1.3 and 1.3 μmol h^{-1} for Ni–Cu/TiO_2 (rutile HS, rutile LS and anatase HS, respectively), which are comparable to that for Ni–Cu/TiO_2 (anatase LS) (1.7 μmol h^{-1}). Although the surface area of TiO_2 (rutile LS) is only *ca.* 1/1000 that of TiO_2 (rutile HS), the catalytic activity of Ni–Cu on these TiO_2 supports is comparable. These results suggest that neither the crystal structures nor the BET surface areas of the TiO_2 supports are insignificant factors to determine the catalytic activity of Ni–Cu/TiO_2.

3. Conclusions

The catalytic activity of Ni–Cu/TiO_2 and Ni–Cu/SiO_2 for H_2 evolution was greatly enhanced by the synergistic effects of

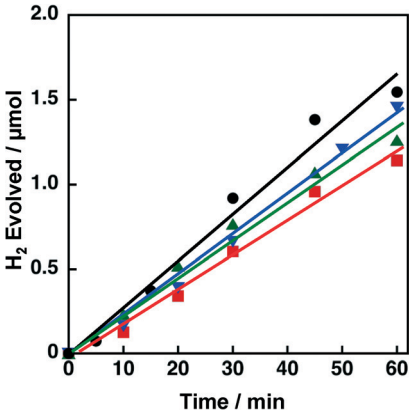

Fig. 12 Time course of H_2 evolution by photoirradiation ($\lambda > 340$ nm) of a mixed suspension (2.0 mL) of a phthalate buffer (pH 4.5) and MeCN [1 : 1 (v/v)] containing $QuPh^+$–NA (8.8×10^{-4} M), NADH (1.0×10^{-3} M) and 3 wt% Ni–Cu supported on TiO_2 (100 mg L^{-1}) with different crystal structures (anatase LS, black circle; rutile HS, blue inverted triangle; anatase HS, red square; rutile LS, green triangle).

Ni and Cu on the photocatalytic H_2 evolution system using 2-phenyl-4-(1-naphthyl)quinolinium ion and NADH as a photocatalyst and an electron donor, respectively. Such a synergistic effect between Ni and Cu was not observed for Ni–Fe and Ni–Co catalysts and for Ni–Cu/SiO_2–Al_2O_3 and Ni–Cu/CeO_2. TEM observation and EDS elemental mapping of Ni–Cu/SiO_2 prepared by the co-impregnation and the sequential impregnation methods suggest that the close location of Ni and Cu is important to achieve the high catalytic activity. The synergistic effect between Ni and Cu was observed in the wide range of Ni contents, Ni/(Ni + Cu), from 30% to 70%. This study has demonstrated that suitable choices of additives, supports, and catalyst preparation methods are all important to achieve highly active H_2 evolution catalysts composed of base metals with synergistic effects.

4. Experimental section

4.1 Materials

All chemicals were obtained from chemical companies and used without further purification. SiO_2 (unshaped, low surface area), TiO_2 (anatase, low surface area) and TiO_2 (anatase, high surface area) were purchased from Sigma-Aldrich. SiO_2 (unshaped, high surface area) was obtained from Merck. Iron nitrate, copper nitrate, nickel nitrate, 2-propanol, hydrochloric acid (37%), sodium aluminate and titanium(IV) chloride were obtained from Wako Pure Chemical Industries. Aqueous ammonia (28%) and β-dihydronicotinamide adenine dinucleotide disodium salt (reduced form) (NADH) were obtained from Tokyo Chemical Industry. Tetraethyl orthosilicate (TEOS) was delivered by Shin-Etsu Chemical. Acetonitrile was obtained from Nacalai Tesque. CeO_2 was provided by Daiichi Kigenso Kagaku Kogyo Co., Ltd. 2-Phenyl-4-(1-naphthyl)quinolinium perchlorate ($QuPh^+$–NA),[42] SiO_2–Al_2O_3,[46] spherical SiO_2,[47] and TiO_2 (rutile, high surface area)[48] were prepared by literature methods. Purified water was provided by using a Millipore DIRECT-Q UV3 water purification system (18.2 MΩ cm).

4.2 Preparation of Ni–Cu supported on metal oxides by a co-impregnation method

A typical procedure for the preparation of metal oxides supporting Ni and Cu by a co-impregnation method is as follows: metal oxide (350 mg) was soaked in an ethanol solution (30 mL) containing $Ni(NO_3)_2{\cdot}6H_2O$ (26.8 mg, 92.2 mmol) and $Cu(NO_3)_2{\cdot}3H_2O$ (20.6 mg, 85.3 mmol) and sonicated for 30 min. The obtained catalyst precursor was dried at 60 °C in an oven and calcined at 350 °C (ramp rate: 5 °C min^{-1}) for 4 h in air. The obtained powder was soaked in an ethanol solution containing $NaBH_4$ to reduce oxides of Cu and Ni before catalysis evaluation.

4.3 Preparation of Ni–Cu supported on TiO_2 and SiO_2 by a sequential impregnation method

A typical procedure for the preparation of TiO_2 and SiO_2 catalysts supporting Cu and Ni by a sequential impregnation method is as follows: TiO_2 or SiO_2 (350 mg) was immersed in an ethanol solution (30 mL) containing $Cu(NO_3)_2{\cdot}3H_2O$ (20.6 mg, 85.3 mmol) and sonicated for 30 min. The obtained catalyst precursor was dried at 60 °C in an oven and calcined at 350 °C (ramp rate: 5 °C min^{-1}) for 4 h in air. Then, the calcined sample was immersed in an ethanol solution (30 mL) containing $Ni(NO_3)_2{\cdot}6H_2O$ (26.8 mg, 92.2 mmol). The obtained slurry was dried and calcined. The obtained powder was soaked in an ethanol solution containing $NaBH_4$ to reduce oxides of Cu and Ni before catalysis evaluation.

4.4 Preparation of Ni–Co and Ni–Fe supported on TiO_2 and SiO_2 by a co-impregnation method

These catalysts were prepared by a co-impregnation method as follows: TiO_2 or SiO_2 (350 mg) was soaked in an ethanol solution (30 mL) containing $Ni(NO_3)_2{\cdot}6H_2O$ (26.8 mg, 92.2 mmol) and $Co(NO_3)_2{\cdot}6H_2O$ (26.8 mg, 92.1 mmol) or $Fe(NO_3)_3{\cdot}9H_2O$ (37.2 mg, 92.1 mmol) and sonicated for 30 min. The obtained catalyst precursor was dried at 60 °C in an oven and calcined at 350 °C (ramp rate: 5 °C min^{-1}) for 4 h in air. The obtained powder was soaked in an ethanol solution containing $NaBH_4$ to reduce oxides of Cu and Ni before catalysis evaluation.

4.5 Preparation of SiO_2–Al_2O_3

SiO_2 was suspended in an aqueous solution (50 mL) containing sodium aluminate (1.3 g, 16 mmol) and stirred for 20 h at room temperature. The precipitate was collected by filtration and dried at 120 °C. The dried sample was calcined at 550 °C (ramp rate: 5 °C min^{-1}) for 6 h in air.

4.6 Preparation of spherical silica

TEOS (18 mL, 80 mmol) was dissolved in a mixture solution of water (31 mL), ethanol (300 mL) and 28% ammonia solution (5.4 mL) and stirred for 4 h at room temperature. After the reaction, the obtained white precipitate was collected by centrifugation (9000 rpm, 10 min) and washed three times with water. The obtained powder was dried at 70 °C in an oven and calcined at 350 °C (ramp rate: 5 °C min^{-1}) for 4 h in air to remove residual ammonia.

4.7 Preparation of TiO_2 (rutile, high surface area)[48]

Titanium(IV) chloride (5.7 g, 30 mmol) was dissolved in a mixture solution of water (100 mL), 2-propanol (200 mL) and hydrochloric acid (10 mL) and refluxed for 20 h at 90 °C. After the solution was cooled to room temperature, the suspension was basified to pH 9 with 28% ammonia solution. The white precipitate was collected by centrifugation (9000 rpm, 10 min) and washed three times with water.

4.8 Preparation of TiO_2 (rutile, low surface area)

TiO_2 (rutile, high surface area) was calcined at 1000 °C (ramp rate: 10 °C min^{-1}) for 3 h in air.

4.9 Transmission electron microscopy (TEM)

The sizes and shapes of SiO_2 supports were determined from bright-field images using a JEOL JEM-2100 that has a thermal field emission gun with an accelerating voltage of 200 kV. The observed samples were prepared by dropping a dispersion of catalysts onto the support and allowing the solvent to evaporate and then scooping up with an amorphous carbon supporting film on a Cu grid. High-angle annular dark-field scanning TEM (HAADF-STEM) images and the energy-dispersive X-ray spectroscopy (EDS) elemental mapping of Ni–Cu/SiO_2 were obtained by using an FEI Titan G2 60-300 with an accelerating voltage of 300 kV. The observed samples were directly put on Mo meshes.

4.10 Catalyst characterisation by powder X-ray diffraction, diffused reflectance UV-vis spectroscopy and dynamic laser scattering

X-ray diffraction patterns were recorded with a Rigaku MiniFlex 600. Incident X-ray radiation was produced by using a Cu X-ray tube operating at 40 kV and 15 mA with a Cu Kα radiation of 1.54 Å. The scanning rate was 2° min^{-1} from 5° to 80° in 2θ. The diffuse reflectance UV-vis spectra were recorded with a Jasco V-670 spectrophotometer equipped with an integrating sphere module (SIN-768). Reflectance obtained for each sample was converted to $f(R_\infty)$ values according to the Kubelka–Munk theory, $f(R_\infty) = (1 - R_\infty)^2/2R_\infty$, where R_∞ is the reflectance of the sample layer. $BaSO_4$ was used for background spectra measurements. Dynamic light scattering (DLS) measurements were performed with a Zetasizer Nano ZS instrument (Malvern Instruments Ltd., USA).

4.11 N_2 adsorption for BET surface area determination

Nitrogen adsorption–desorption at 77 K was performed with a Belsorp-mini (BEL Japan, Inc.) within a relative pressure range from 0.01 to 101.3 kPa. A sample mass of ~100 mg was used for adsorption analysis after pretreatment at 120 °C for 1 h under vacuum conditions and kept in N_2 atmosphere until N_2 adsorption measurements. The samples were exposed to a mixed gas of He and N_2 with a programmed ratio, and an adsorbed amount of N_2 was calculated from the change in pressure in a cell after reaching the equilibrium (at least 5 min). The surface area of each catalyst was determined by the Brunauer–Emmett–Teller (BET) method for multiple N_2 adsorption amounts under the conditions of partial pressure less than 0.3.

4.12 Photocatalytic H_2 evolution

A mixed solution (2.0 mL) of a phthalate buffer (pH 4.5) and MeCN [1 : 1 (v/v)] containing $QuPh^+$–NA (0.88 mM), NADH (1.0 mM) and an H_2 evolution catalyst was flushed with N_2 gas. The solution was then irradiated for a certain time with a xenon lamp (Ushio Optical, Model X SX-UID 500X AMQ) through a colour filter glass (Asahi Techno Glass L39) transmitting $\lambda > 340$ nm at room temperature. After 1 min of stirring in the dark, the gas in the headspace was analysed by Shimadzu GC-14B gas chromatography (detector: TCD, column temperature: 50 °C, column: active carbon with the particle size of 60–80 mesh, carrier gas: N_2 gas) to determine the amount of evolved H_2.

Acknowledgements

This work was supported by grants-in-aid (no. 24350069 and 25600025) for Scientific Research from the Japan Society for the Promotion of Science (JSPS), an ALCA project from the Japan Science and Technology Agency (JST). We sincerely acknowledge the Research Centre for Ultra-Precision Science & Technology, Osaka University, for TEM measurements.

Notes and references

1 H. B. Gray, *Nat. Chem.*, 2009, **1**, 7–7.
2 D. G. Nocera, *Acc. Chem. Res.*, 2012, **45**, 767–776.
3 (*a*) Z. Han and R. Eisenberg, *Acc. Chem. Res.*, 2014, **47**, 2537–2544; (*b*) K. S. Joya, Y. F. Joya, K. Ocakoglu and R. van de Krol, *Angew. Chem., Int. Ed.*, 2013, **52**, 10426–10437.
4 F. E. Osterloh, *Chem. Soc. Rev.*, 2013, **42**, 2294–2320.
5 (*a*) T. Hisatomi, J. Kubota and K. Domen, *Chem. Soc. Rev.*, 2014, **3**, 1486–1503; (*b*) K. Maeda, *ACS Catal.*, 2013, **3**, 1486–1503; (*c*) K. Maeda and K. Domen, *Chem. Mater.*, 2010, **22**, 612–623.
6 R. Abe, in *New and Future Developments in Catalysis: Solar Photocatalysis*, Elsevier B.V., 2013, pp. 341–370.
7 (*a*) A. Kudo and Y. Miseki, *Chem. Soc. Rev.*, 2009, **38**, 253–278; (*b*) Y. Miseki and A. Kudo, *ChemSusChem*, 2011, **4**, 245–251.

8 (*a*) H. Hagiwara, M. Watanabe, T. Daio, S. Ida and T. Ishihara, *Chem. Commun.*, 2014, **50**, 12515–12518; (*b*) H. Hagiwara, T. Inoue, S. Ida and T. Ishihara, *Phys. Chem. Chem. Phys.*, 2011, **13**, 18031–18037.

9 (*a*) K. Mori, J. Aoyama, M. Kawashima and H. Yamashita, *Dalton Trans.*, 2014, **43**, 10541–10547; (*b*) T. Kamegawa, S. Matsuura, H. Seto and H. Yamashita, *Angew. Chem., Int. Ed.*, 2013, **52**, 916–919.

10 (*a*) Y. Horiuchi, T. Toyao, M. Takeuchi, M. Matsuoka and M. Anpo, *Phys. Chem. Chem. Phys.*, 2013, **15**, 13243–13253; (*b*) T. Toyao, M. Saito, S. Dohshi, K. Mochizuki, M. Iwata, H. Higashimura, Y. Horiuchi and M. Matsuoka, *Chem. Commun.*, 2014, **50**, 6779–6781.

11 S. Fukuzumi and Y. Yamada, *ChemSusChem*, 2013, **6**, 1834–1847.

12 V. Artero and M. Fontecave, *Chem. Soc. Rev.*, 2013, **42**, 2338–2356.

13 (*a*) J. J. Concepcion, R. L. House, J. M. Papanikolas and T. J. Meyer, *Proc. Natl. Acad. Sci. U. S. A.*, 2012, **109**, 15560–15564; (*b*) A. K. Vannucci, L. Alibabaei, M. D. Losego, J. J. Concepcion, B. Kalanyan, G. N. Parsons and T. J. Meyer, *Proc. Natl. Acad. Sci. U. S. A.*, 2013, **110**, 20918–20922.

14 A. J. Cowan and J. R. Durrant, *Chem. Soc. Rev.*, 2013, **42**, 2281–2293.

15 S. Fukuzumi, K. Ohkubo and T. Suenobu, *Acc. Chem. Res.*, 2014, **47**, 1455–1464.

16 M. D. Kärkäs, E. V. Johnston, O. Verho and B. Åkermark, *Acc. Chem. Res.*, 2014, **47**, 100–111.

17 J. R. McKone, N. S. Lewis and H. B. Gray, *Chem. Mater.*, 2014, **26**, 407–414.

18 (*a*) H. Ozawa and K. Sakai, *Chem. Commun.*, 2011, **47**, 2227–2242; (*b*) M. Kobayashi, S. Masaoka and K. Sakai, *Angew. Chem., Int. Ed.*, 2012, **51**, 7431–7434.

19 (*a*) J. P. Prieto, *EPA Newsl.*, 2013, **84**, 85–86; (*b*) J. M. Thomas, *Energy Environ. Sci.*, 2014, **7**, 19–19.

20 (*a*) M. Wang, L. Chen and L. Sun, *Energy Environ. Sci.*, 2012, **5**, 6763–6778; (*b*) N. Wang, M. Wang, L. Chen and L. Sun, *Dalton Trans.*, 2013, **42**, 12059–12071.

21 (*a*) M. Grätzel, *Acc. Chem. Res.*, 1981, **14**, 376–384; (*b*) J. Kiwi, K. Kalyanasundaram and M. Grätzel, *Struct. Bonding*, 1982, **49**, 37–125.

22 S. Fukuzumi, D. Hong and Y. Yamada, *J. Phys. Chem. Lett.*, 2013, **4**, 3458–3467.

23 S. Fukuzumi, Y. Yamada, T. Suenobu, K. Ohkubo and H. Kotani, *Energy Environ. Sci.*, 2011, **4**, 2754–2766.

24 (*a*) H. Kotani, R. Hanazaki, K. Ohkubo, Y. Yamada and S. Fukuzumi, *Chem. – Eur. J.*, 2011, **17**, 2777–2785; (*b*) H. Kotani, K. Ohkubo, Y. Takai and S. Fukuzumi, *J. Phys. Chem. B*, 2006, **110**, 24047–24053; (*c*) H. Kotani, T. Ono, K. Ohkubo and S. Fukuzumi, *Phys. Chem. Chem. Phys.*, 2007, **9**, 1487–1492.

25 (*a*) Y. Yamada, T. Miyahigashi, K. Ohkubo and S. Fukuzumi, *Phys. Chem. Chem. Phys.*, 2012, **14**, 10564–10571; (*b*) Y. Yamada, H. Tadokoro and S. Fukuzumi, *RSC Adv.*, 2013, **3**, 25677–25680; (*c*) Y. Yamada, A. Nomura, H. Tadokoro and S. Fukuzumi, *Catal. Sci. Technol.*, 2014, DOI: 10.1039/C4CY01005A.

26 S. Harinipriya and M. V. Sangaranarayanan, *Langmuir*, 2002, **18**, 5572–5578.

27 P. S. Bassi, Gurudayal, L. H. Wong and J. Barber, *Phys. Chem. Chem. Phys.*, 2014, **16**, 11834–11842.

28 Y. Yamada, T. Miyahigashi, H. Kotani, K. Ohkubo and S. Fukuzumi, *J. Am. Chem. Soc.*, 2011, **133**, 16136–16145.

29 Y. Yamada, T. Miyahigashi, H. Kotani, K. Ohkubo and S. Fukuzumi, *Energy Environ. Sci.*, 2012, **5**, 6111–6118.

30 Y. Yamada, S. Shikano and S. Fukuzumi, *J. Phys. Chem. C*, 2013, **117**, 13143–13152.

31 S. K. Beaumont, S. Alayoglu, V. V. Pushkarev, Z. Liu, N. Kruse and G. A. Somorjai, *Faraday Discuss.*, 2013, **162**, 31–44.

32 (*a*) B. R. Greenhalgh, S. M. Kuznicki and A. E. Nelson, *Appl. Catal., A*, 2007, **327**, 189–196; (*b*) D. Gulkova and M. Zdrazil, *Collect. Czech. Chem. Commun.*, 1999, **64**, 735–746; (*c*) J. Hermannsdoerfer, M. Friedrich, N. Miyajima, R. Q. Albuquerque, S. Kuemmel and R. Kempe, *Angew. Chem., Int. Ed.*, 2012, **51**, 11473–11477; (*d*) M. P. M. Kaninski, S. M. Miulovic, G. S. Tasic, A. D. Maksic and V. M. Nikolic, *Int. J. Hydrogen Energy*, 2011, **36**, 5227–5235; (*e*) M. A. Keane, S. Gomez-Quero, F. Cardenas-Lizana and W. Shen, *ChemCatChem*, 2009, **1**, 270–278; (*f*) S. A. Nikolaev and V. V. Smirnov, *Catal. Today*, 2009, **147**, 336–341; (*g*) A. K. Singh and Q. Xu, *ChemCatChem*, 2013, **5**, 3000–3004; (*h*) J. Zhang, J.-O. Mueller, W. Zheng, D. Wang, D. Su and R. Schlögl, *Nano Lett.*, 2008, **8**, 2738–2743; (*i*) Q.-L. Zhu, J. Li and Q. Xu, *J. Am. Chem. Soc.*, 2013, **135**, 10210–10213.

33 S.-Z. Kang, L. Chen, X. Li and J. Mu, *Appl. Surf. Sci.*, 2012, **258**, 6029–6033.

34 (*a*) Y. Zhang, W. Huang, S. E. Habas, J. N. Kuhn, M. E. Grass, Y. Yamada, P. Yang and G. A. Somorjai, *J. Phys. Chem. C*, 2008, **112**, 12092–12095; (*b*) H. Yen and F. Kleitz, *J. Mater. Chem. A*, 2013, **1**, 14790–14796.

35 (*a*) S. A. Khromova, A. A. Smirnov, O. A. Bulavchenko, A. A. Saraev, V. V. Kaichev, S. I. Reshetnikov and V. A. Yakovlev, *Appl. Catal., A*, 2014, **470**, 261–270; (*b*) J. Ashok, P. S. Reddy, G. Raju, M. Subrahmanyam and A. Venugopal, *Energy Fuels*, 2009, **23**, 5–13; (*c*) L.-C. Chen and S. D. Lin, *Appl. Catal., B*, 2011, **106**, 639–649; (*d*) S. K. Saraswat and K. K. Pant, *J. Nat. Gas Sci. Eng.*, 2013, **13**, 52–59; (*e*) A. J. Vizcaino, A. Carrero and J. A. Calles, *Int. J. Hydrogen Energy*, 2007, **32**, 1450–1461.

36 S. Ma, Y. Tan and Y. Han, *J. Ind. Eng. Chem.*, 2011, **17**, 723–726.

37 Y. Echegoyen, I. Suelves, M. J. Lázaro, R. Moliner and J. M. Palacios, *J. Power Sources*, 2007, **169**, 150–157.

38 M. Kang, M. W. Song, T. W. Kim and K. L. Kim, *Can. J. Chem. Eng.*, 2002, **80**, 63–70.

39 (*a*) B. M. Reddy, K. N. Rao and P. Bharali, *Ind. Eng. Chem. Res.*, 2009, **48**, 8478–8486; (*b*) Y. Li, Q. Fu and M. Flyzani-Stephanopoulos, *Appl. Catal., B*, 2000, **27**, 179–191.

40 P. López, G. Mondragón-Galicia, M. E. Espinosa-Pesqueira, D. Mendoza-Anaya, M. E. Fernández, A. Gómez-Cortés, J. Bonifacio, G. Martínez-Barrera and R. Pérez-Hernández, *Int. J. Hydrogen Energy*, 2012, **37**, 9018–9027.

41 (*a*) H.-J. Kim, L. Lu, J.-H. Kim, C.-H. Lee, T. Hyeon, W. Choi and H.-I. Lee, *Bull. Korean Chem. Soc.*, 2001, **22**, 1371–1374; (*b*) M. Lazaro, Y. Echegoyen, C. Alegre, I. Suelves, R. Moliner and J. Palacios, *Int. J. Hydrogen Energy*, 2008, **33**, 3320–3329; (*c*) P. Li, J. Liu, N. Nag and P. A. Crozier, *J. Catal.*, 2009, **262**, 73–82; (*d*) N. Riaz, F. K. Chong, B. K. Dutta, Z. B. Man, M. S. Khan and E. Nurlaela, *Chem. Eng. J.*, 2012, **185–186**, 108–119; (*e*) N. Riaz, F. K. Chong, Z. B. Man, M. S. Khan and B. K. Dutta, *Ind. Eng. Chem. Res.*, 2013, **52**, 4491–4503.

42 H. Kotani, K. Ohkubo and S. Fukuzumi, *Faraday Discuss.*, 2012, **155**, 89–102.

43 S. Fukuzumi, H. Kotani, K. Ohkubo, S. Ogo, N. V. Tkachenko and H. Lemmetyinen, *J. Am. Chem. Soc.*, 2004, **126**, 1600–1601.

44 D. D. Wagman, W. H. Evans, V. B. Parker, R. H. Schumm, I. Halow, S. M. Bailey, K. L. Churney and R. L. Nuttall, *J. Phys. Chem. Ref. Data*, 1982, **11**, 1–392.

45 (*a*) H. G. El-Shobaky, *Appl. Catal., A*, 2004, **278**, 1–9; (*b*) H. G. El-Shobaky and Y. M. Fahmy, *Appl. Catal., B*, 2006, **63**, 168–177.

46 M. L. D. A. Martinez, F. A. L. D'Amicis, A. R. Beltramon, M. B. G. Costa and O. A. Anunziata, *Mater. Res. Bull.*, 2011, **46**, 1011–1021.

47 W. Stöber and A. Fink, *J. Colloid Interface Sci.*, 1968, **26**, 62–69.

48 B. I. Lee, X. Wang, R. Bhave and M. Hu, *Mater. Lett.*, 2006, **60**, 1179–1183.